



# Compositional profiling and molecular docking studies of *Eucalyptus polybrachtea* essential oil against mucormycosis and aspergillosis

ARUN DEV SHARMA \*, INDERJEET KAUR, AMRITA CHAUHAN

Post Graduate Department of Biotechnology, Lyallpur Khalsa College Jalandhar, Jalandhar, Punjab, India

Received: 17 August 2022; revised: 6 January 2023; accepted: 12 April 2023

## Abstract

Essential oil (EO) from *Eucalyptus polybrachtea* is used as complementary and traditional medicine worldwide. The present study aimed at compositional profiling of EO and molecular docking of EO's bioactive compound 1,8 cineole against fungal enzymes involved in the riboflavin synthesis pathway, namely riboflavin synthase (RS), riboflavin biosynthesis protein RibD domain-containing protein (RibD), and 3,4-dihydroxy-2-butanone 4-phosphate synthase (DBPS) as apposite sites for drug designing against aspergillosis and mucormycosis, and *in vitro* confirmation. The compositional profile of EO was completed by GC-FID analysis. For molecular docking, the Patchdock tool was used. The ligand-enzyme 3-D interactions were examined, and ADMET properties (absorption, distribution, metabolism, excretion, and toxicity) were calculated. GC-FID discovered the occurrence of 1,8 cineole as a major component in EO, which was subsequently used for docking analysis. The docking analysis revealed that 1,8 cineole actively bound to RS, RibD, and DBPS fungal enzymes. The results of the docking studies demonstrated that the ligand 1,8 cineole exhibited H-bond and hydrophobic interactions with RS, RibD, and DBPS fungal enzymes. 1,8 cineole obeyed Lipinsky's rule and exhibited adequate bioactivity. Wet-lab authentication was achieved by using three fungal strains: *Aspergillus niger*, *Aspergillus oryzae*, and *Mucor sp.* Wet lab results indicated that EO was able to inhibit fungal growth.

**Key words:** aspergillosis, mucormycosis, eucalyptus oil, herbal drug

## Introduction

During the COVID-19 pandemic, many co-infections were reported worldwide (Alanio et al., 2020; Chang et al., 2020). Among all, opportunistic fungal infections such as mucormycosis and aspergillosis are caused by common fungal molds such as *Aspergillus* and *Mucor spp.*, which are responsible for a significant morbidity and mortality rate of 68% (Ventoulis et al., 2020). In the past, scientists believed that fungal infections primarily occurred in individuals with severely weakened immune systems (Song et al., 2020). However, fungal infections such as aspergillosis have increasingly been reported in patients with severe respiratory infections caused by viruses, including influenza (Gangneux et al., 2020; Lans-

bury et al., 2020; Hoenig et al., 2022). A recent systematic review indicated that the frequency of fungal co-infections among patients with COVID-19 was 49.7%, 23.2%, 19.8%, 6.6%, and 0.5% in Asia, America, Europe, Africa, and Australia, respectively (Seyedjavadi et al., 2022). It was reported that COVID-19 likely augmented the risk of fungal infections due to its effect on the immune system and because treatments for COVID-19 (like steroids and other drugs) can weaken the body's defenses against fungi. These fungal infections pose a serious health risk for severely immune-compromised individuals treated with the uncontrolled use of steroids, hence termed "COVID-19-associated mucormycosis/aspergillosis" (CAM/CAA) (John et al., 2021). The indi-

\* Corresponding author: Post Graduate Department of Biotechnology, Lyallpur Khalsa College Jalandhar, Jalandhar, Punjab, India; e-mail: arundevsharma47@gmail.com

cations related to aspergillosis include a running nose, stiffness, coughing with blood, pain, fever, and reduced sense of smell (Schweer et al., 2014). Symptoms associated with mucormycosis include blackish discoloration around the nose, stuffy and bleeding nose, black crusts oozing out from the nose, loosening of teeth and jaw, numbness and one-sided facial pain, swelling of the eyes, blurred vision, and problems with the respiratory system (Garg et al., 2021).

Due to the clinical limitations of fungicidal agents, like high price, inevitable toxicities, and fungal drug resistance, the search for novel antifungal drugs is a prerequisite (Cuenca-Estrella, 2014). Previous studies have proposed that bioactive molecules that act as enzymatic antifungal inhibitors can be used as therapeutic drugs to mitigate fungal infections (Chen et al., 2020). Riboflavin, a yellow pigment also known as vitamin B<sub>2</sub>, is a key micronutrient that serves as a universal precursor to coenzymes flavin adenine dinucleotide and flavin mononucleotide. It is essential for biochemical reactions in all living cells, including bacteria and fungi (Averianova et al., 2020). Many naturally occurring flavinogenic microorganisms like bacteria and fungal species are capable of synthesizing riboflavin (Averianova et al., 2020). These flavocoenzymes also play a role in the metabolism of lipids, proteins, carbohydrates, and ketone bodies, which are sources of energy for living organisms, thereby affecting the growth and viability of living cells. Unlike animals, fungi can synthesize this essential component themselves, leading to the conclusion that targeting riboflavin production is a promising novel strategy against fungal infections (Demuyser et al., 2020). Among the various enzymes involved in the riboflavin biosynthetic pathway, riboflavin synthase (RS) catalyzes the final step in the biosynthesis of riboflavin, while 3,4-dihydroxy-2-butanone 4-phosphate synthase (DBPS) and riboflavin biosynthesis protein domain-containing protein (RibD) are major proteins implicated in the initiation of the riboflavin synthesis pathway (Jain et al., 2013). Since these proteins are essential in fungi but absent in humans, they can be effective targets for therapeutic interventions (Madhavan et al., 2022). Consequently, such proteins can serve as excellent drug target sites for antifungal drugs. This study postulates the viewpoint that bioactive compounds like 1,8 cineole have the potential to combat fungal infections by targeting RS, RibD, and DBPSG.

1,8-Cineole (eucalyptol), one of the most common monoterpenes, is an achiral aromatic component found in many plants, including *Eucalyptus* leaves. 1,8-cineole is a major bioactive component of *Eucalyptus* essential oil (EO) in all *Eucalyptus* spp. (Tyagi et al., 2011). 1,8-cineole is known for its mucolytic, broncholytic, and anti-inflammatory properties, making it useful in the treatment of respiratory tract diseases. Previous studies have documented the antifungal potential of *Eucalyptus* leaf extracts against *Candida albicans* and dermatophytes (Sebei et al., 2015). However, due to the complexity of *Eucalyptus* EO, its antifungal mechanism of action is still not completely understood (Elaiissi et al., 2011). We present the viewpoint that due to the abundance of 1,8-cineole in EO from *Eucalyptus polybrachtea* it may have the potential to mitigate aspergillosis and mucormycosis. Therefore, the aim of the present study was to investigate the 3D docking of 1,8-cineole against RS, RibD, and DBPS and perform wet-lab authentication. However, the potential of 1,8-cineole against aspergillosis and mucormycosis is still a matter of speculation. This study introduces new ideas for the potential identification of key antifungal drugs during COVID-19 treatment.

## Material and methods

### GC-FID analysis of EO

EO was extracted from fresh leaves of *Eucalyptus polybrachtea*, which naturally grow in the nearby areas of Lyallpur Khalsa College, Jalandhar, India. The authentication of *Eucalyptus polybrachtea* was performed by Dr. Upma from Botany Department, Lyallpur Khalsa College, Jalandhar. A specimen voucher with BT103 number was deposited in the Department of Biotechnology, Lyallpur Khalsa College, Jalandhar, India. Hydrodistillation method was used for extraction of EO following the method outlined by Sebei et al. (2015). A clevenger-type apparatus (Borosil, India) was employed for the extraction process. To identify the bioactive compounds in EO, a GC-FID study was carried out (GC-FID, Chemtron 2045). The specifications of the column were as follows: 2 m long, stainless steel having 10% OV-17 on 80–100% mesh Chromosorb W (HP). Nitrogen was used as the carrier gas at a flow rate of 35 ml/min. A 0.2 µl EO sample was used. The detector and injector temperatures were set at 220 and 270 °C, respectively. The oven ramping conditions were initially maintained at 100 °C and ramped to 2100 °C at 3 °C/min. Bioactive consti-

tents in EO were identified by comparing the relative retention times (RT) of the GC-FID spectra of the EO with authentic standards (eucalyptol, citral, eugenol and geraniol, Sigma-Aldrich (St. Louis, MO, USA)) and literature data.

#### **Ligand preparation**

For fungal receptors, including RS with Pdb id 1I8D, RibD with Pdb id 7DS0, and DBPS with Pdb id 1G57, 1,8-cineole was used as a ligand. To build the 3D structure of the ligand, the SMILES notation of 1,8-cineole (PubChem CID: 2758) was retrieved from the NCBI-PubChem database. The structure was built by using UCSF-chimera. To generate the 3D structure, the SMILES notation was uploaded into the built-in tool "built structure" in UCSF-chimera, and the job was executed. The resulting file was saved as "pdb" and used for further analysis in docking.

#### **Molecular docking**

The crystal structures of RS, RibD, and DBPS fungal enzymes were obtained from PDB (<https://www.rcsb.org/>). Before the docking analysis, the target enzymes were prepared by removing selected H<sub>2</sub>O molecules, cofactors, and co-crystallized ligands, and undergoing energy minimization. All protein target structures were prepared by means of the dock prep set up in UCSF-chimera. The process optimized bond length, charged anomalies, and corrected atomic structure. The PatchDock tool was used for docking ligands over RS, RibD, and DBPS (<https://bioinfo3d.cs.tau.ac.il/PatchDock/>). Both receptors and ligand molecules were uploaded as "pdb files" to the PatchDock and docking was performed with default Clustering RMSD 4.0. The resulting complex of the topmost model with the maximum docking score generated by PatchDock was saved as "pdb" file and used for further analysis. To analyze the 3D interactions in docked complexes, the Plip tool (<https://plip-tool.biotec.tu-dresden.de/plip-web/plip/index>) was used. The pdb file of the docked complex was uploaded to the Plip server, and the job was executed.

#### **Drug-likeness and toxicity**

ADMET (absorption, metabolism, toxicity, and excretion), drug likeness, physiochemical properties, and pharmacokinetics were studied using the SWISSADME tool (<http://www.swissadme.ch/>). The pdb file of the doc-

ked complex was uploaded to the SWISSADME server, the job was executed, and the final results were retrieved. ProTox-II was used for the determination of toxicity profile, oral toxicity, hepatotoxicity, immunotoxicity, mutagenicity, carcinotoxicity, cytotoxicity, and analysis ([http://tox.charite.de/prottox\\_II](http://tox.charite.de/prottox_II)). The pdb file of the docked complex was uploaded to ProTox-II server, and the job was executed. The bioactivity potential of 1,8 cineole was studied by using the web-based Molinspiration tool (<https://www.molinspiration.com/cgi-bin/properties>). The pdb file of the docked complex was uploaded to the Molinspiration server, and the job was executed.

#### **Active sites prediction of proteins**

To identify the cavities and determine their dimensions on the 3D active sites of the fungal receptors, the CASTp web tool was employed. All structures in "pdb" format were uploaded to the server and prediction was executed with a probe radius value of 1.4 Å. The 3D structures were viewed inside the tool, and the data was noted.

#### **In vitro antifungal activity of EO**

The antifungal activity of EO was determined using the poison food technique described by Gakuubi et al. (2017). The anti-aspergillosis and antimucormycosis potential of EO were tested against the fungal strains *Aspergillus niger* (MTCC 277), *Aspergillus oryzae* (MTCC 343), and *Mucor* sp. (MTCC 3473). All microorganisms were bought from IMTECH (Institute of Microbial Technology, Chandigarh, India). To conduct the antifungal activity assay, the EO was added to autoclaved potato dextrose agar (PDA) agar medium (HiMedia) at concentrations of 50 µl and 100 µl. The mixture was then poured into sterile Petri plates (8 cm in diameter) and allowed to solidify at ~37°C for 3 hrs. Mycelial fungal discs (8 mm) were taken from fungal plates with the help of a sterile cork borer and aseptically placed on Petri plates. The plates were then incubated for 15 days at 29°C. As a positive control, antibiotic discs containing 25 mg ketoconazole (Leford Pvt Ltd, India) were used. MGI (Mycelial growth inhibition) was premeditated by using the following equation:

$$(MGI\%) = DC - DT/DC \times 100,$$

where DC and DT are the diameters of the control and test colonies. The antifungal activity experiments were performed in triplicate.

## Results and discussion

### GC-FID profiling

The aroma profile of EO components identified by GC-FID is displayed in Figure 1 and Table 1. GC-FID analysis of EO displayed the incidence of 39 peaks, including major and minor ones. The bioactive components identified in EO were eucalyptol (1,8 cineole) (13%),  $\alpha$ -pinene (10%), Trans-Geraniol (7.4%), Beta-myrcene (4.5%) and citral (2.9%). As reported in the literature, *Eucalyptus* EO is predominant in eucalyptol (1,8 cineole) (Raho et al., 2012). Due to the presence of this bioactive molecule, eucalyptus EO has tremendous applications in health- and medical-related research (Kushwaha et al., 2018). The characteristic odor of EO oil is due to its high alcohol content, mainly 1,8 cineole, and small but varying amounts of esters associated with geraniol. Due to these bioactive molecules, EO has a rose-like aroma and has immense applications in high-grade perfumery, cosmetics, flavoring and aromatherapy, fragrances, soaps, detergents, toiletry, tobacco products, and pharmaceutical industries (Lawrence et al., 2012; Bhatnagar, 2018). Therefore, 1,8 cineole was selected as a ligand for docking studies against fungal enzyme receptors.

### Molecular docking

Structure-based drug design (SBDD) is a widely utilized *in silico* technique for drug development, relying on 3-D structures (Singh et al., 2016). *In silico* docking has helped investigators to screen 3D conformations and possible interactions of bioactive components against receptors (Barcellos et al., 2019). The present study aimed at docking 1,8 cineole, a bioactive molecule from the EO, as a key fungal inhibitor candidate against RS, RibD, and DBPSG. From docking analysis, it was apparent that the ligand efficiently docked with RS, RibD, and DBPSG fungal enzymes. The 3D docking results depicted strong binding of fungal enzymes with 1,8 cineole (Table 2), as apparent from its docking scores. Among all receptors, 1,8 cineole depicted strong binding with RS, exhibiting a docking score of 18010. The docking score for RibD was 13132, and for DBPS it was 16790.

Figure 2A, Figure 2B, and Figure 2C present the 3D models depicting the docking poses, hydrophobicity view, and 2D/3D interactions of 1,8 cineole with RS, RibD, and DBPSG fungal enzymes, respectively. The

Table 1. Chemical composition of essential oil from *Eucalyptus polybrachtea*

RT [min]	Compound	Concentration [%]
0.5	citral	2.9
3.7	$\alpha$ -pinene	10.4
5.8	$\beta$ -pinene	1.6
6.9	1,8 cineole	10.1
9.6	1,8 cineole	3.1
16.5	sabinene	3.2
18.0	beta-myrcene	4.5
19.6	terpinolene	1.1
20.8	limonene	0.5
21.8	$\gamma$ -terpinene	0.8
22.9	4-carene	1.1
25.4	pinocarveol	0.9
26.3	4-terpineol	1.2
28.5	$\alpha$ -terpineol	2.4
30.2	$\alpha$ -pinene epoxide	1.2
31.8	dehydro- $\rho$ -cymene	1.1
33.1	cis-limonene oxide	2.1
35.4	linalool	1.7
38.0	fenchyl alcohol	1.0
40.0	eugenol	1.0
43.3	eugenol	0.59
45.2	carvone	2.1
48.2	trans-geraniol	7.4
53.1	unknown	5.8

hydrophobicity view reveals that ligands are firmly bound within the binding pocket of receptors. In the case of RS, 1,8 cineole docks between two monomers in the homotrimer structure of RS. With RibD, 1,8 cineole docks with the C-terminal domain of the RibD protein. These findings are in agreement with previous studies reporting docking interactions of EO-based bioactives from plants *Trachyaspermum ammi*, *Thymus vulgaris*, and *Boswellia carteri* with fungal enzymes such as Ras-like GTP-binding protein (RHO1), Mitogen-activated protein kinase (FMK1), Histone H3-K4 methyltransferase (SET7) from *Fusarium oxysporum* (Biswal et al., 2019; Omar et al., 2021). The authors reported that bioactives from *Thymus vulgaris* EO, such as carvacrol,  $\alpha$ -thujene, and thymol compounds, bound to the active sites of

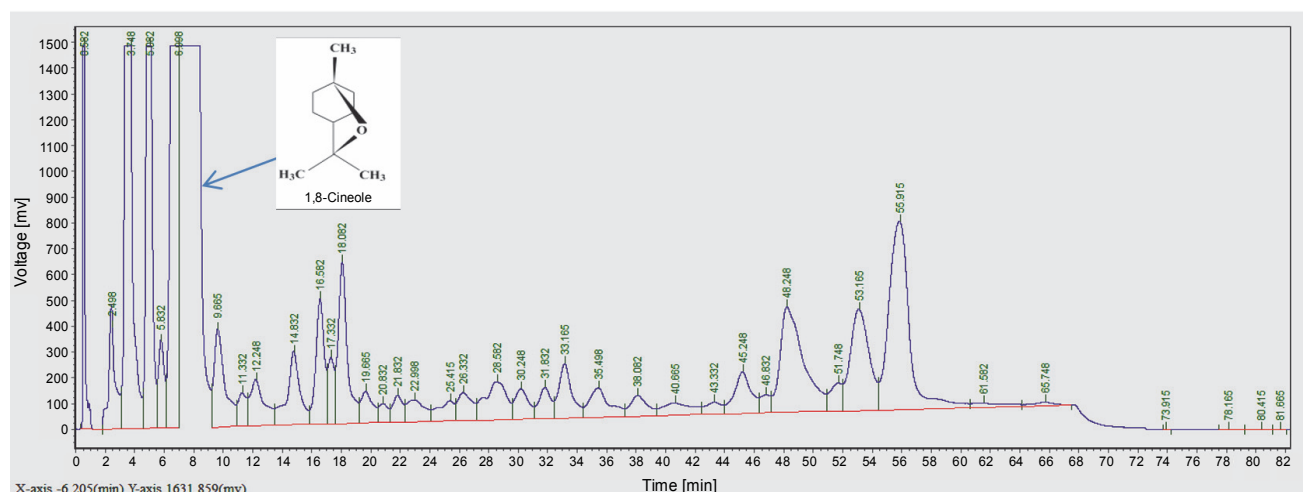
Fig. 1. GC-FID profile of *Eucalyptus polybrachtea* essential oil

Table 2. Molecular docking of fungal receptors with 1,8 cineole

Fungal receptor [ligand name]	Docking score				Interacting residues within 4 Å° radius	
	score	area	ACE	transformation	hydrophobic interactions	hydrogen bonds
Riboflavin synthase (RS) [Pdb id: 1I8D]	18010	3373.10	186.00	1.06 -1.14 -0.97 -87.66 46.68 12.52	LEU 304, TRP 363, 373	ASN 146
Riboflavin biosynthesis protein RibD [Pdb id: 7DS0]	13132	1634.90	268.26	1.22 0.82 -2.61 -54.58 17.08 -34.58	LEU 304, TRP 363, 373	ASN 146
3,4-Dihydroxy-2-butanone-4- phosphate synthase (DBPS) [Pdb id: 1G57]	16790	2207.90	399.30	2.78 -0.45 -1.44 162.75 32.34 -14.95	LEU 304, TRP 363, 373	ASN 146

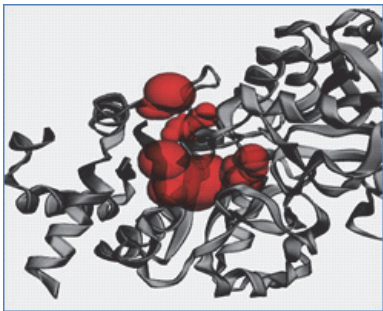
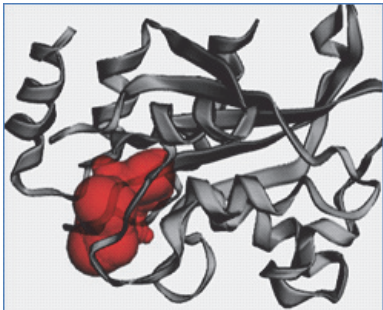
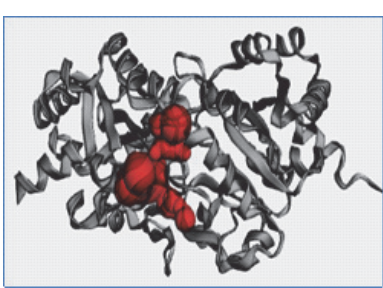
pathogenic proteins with binding affinities ranging from  $-4.1$  to  $-6.9$  kcal/mol. (Omar et al., 2021) Similarly, the nonacosane and tetratriacontane ligands from *Boswellia carteri* EO bound to pathogenic proteins with a binding energy that varied from  $-5.2$  to  $-5.9$  kcal/mol (Omar et al., 2021). In *Trachyspermum ammi* EO, major bioactive compound ligustilide had the lowest free binding energy of  $-5.75$  kcal/mol, followed by cedrane with  $-5.20$  kcal/mol (Biswal et al., 2019). These studies further emphasize the potential of EO as an effective source of antifungal compounds.

With receptors, ligands can form H-bonds or hydrophobic bonds, which designate the affinity of the ligand with the receptor (Lima et al., 2019). Hence, docking interactions of 1,8 cineole with RS, RibD, and DBPS were further evaluated. It was observed that 1,8 cineole forms both H-bond and hydrophobic interactions with RS, RibD, and DBPS. With all fungal receptors, hydro-

phobic interactions were detected via LEU 304, TRP 363, and TRP 373 (Fig. 2). Additionally, 1,8 cineole formed a hydrogen bond with ASN146 in all receptors CASTp active sites prediction quantified interacting residues in the active site cavities of RS, RibD, and DBPS receptors (Table 3). In RS enzymes, a main pocket was documented with a volume of  $214 \text{ \AA}^2$  and an area of  $376 \text{ \AA}^2$ . For RibD, a volume of  $158 \text{ \AA}^2$  and an area of  $237 \text{ \AA}^2$ , and DBPS a volume of  $214 \text{ \AA}^2$  and an area of  $376 \text{ \AA}^2$  were noticed. Based on these observations, it can be concluded that 1,8 cineole exhibits good affinity to all fungal enzymes. It is hypothesized that upon binding with the ligand, RS, RibD, and DBPS undergo conformational changes and become closed. All these events inhibit fungal viability, mitigating the infectivity of the fungus in the host cell. Similar *in silico* results highlighting hydrogen and hydrophobic interactions of bioactive components from *Trachyspermum*



Table 3. Active site analysis of protein target structures

Fungal receptor	3D model	Interacting active site residues	Cavity	
			area (SA)	volume (SA)
Riboflavin synthase (RS)		33, ASP, 38, GLU, 39, ASN, 40, GLU, 42, ASP, 65, ILE, 67, CYS, 89, SER, 90, ALA, 91, TYR, 93, THR, 95, PHE, 140, LEU, 150, ARG, 151, GLY, 153, HIS, 154, THR, 172, LEU, 174, GLU, 181, THR, 182, MET, 183, ALA, 184, ARG, 202, ILE, 100, GLU, 100, GLU, 100, GLU, 101, ALA, 102, ALA, 105, VAL, 106, THR, 106, THR, 107, THR, 109, VAL, 109, VAL, 110, SER, 113, ASP, 132, ASN, 134, PRO, 135, GLY, 136, HIS, 136, HIS,	376.234	214.570
Riboflavin biosynthesis protein RibD		24, THR, 25, ASN, 26, PHE, 28, VAL, 53, THR, 54, MET, 59, ASN, 60, THR, 61, HIS, 62, ALA, 63, GLU, 97, VAL, 99, MET, 100, GLU, 101, PRO, 102, CYS, 104, LYS, 105, ARG, 106, LEU, 107, SER, 112, CYS, 136, GLU, 137, PRO	237.766	158.102
3,4-Dihydroxy-2-butanone-4-phosphate synthase (DBPS)		33, ASP, 38, GLU, 39, ASN, 40, GLU, 42, ASP, 67, CYS, 89, SER, 90, ALA, 91, TYR, 93, THR, 95, PHE, 140, LEU, 150, ARG, 151, GLY, 152, GLY, 153, HIS, 154, THR, 172, LEU, 174, GLU, 181, THR, 182, MET, 183, ALA, 184, ARG, 202, ILE, 100, GLU, 101, ALA, 105, VAL, 106, THR, 107, THR, 109, VAL, 110, SER, 113, ASP, 132, ASN, 134, PRO, 135, GLY, 136, HIS	376.234	214.570

*ammi* essential oil as antifungal agents have been reported. (Biswal et al., 2019). The authors described fifteen active compounds and their interactions with candidapepsin-1. Among all the compounds, ligustilide exhibited the lowest free binding energy of  $-5.75$  kcal/mol against the candidapepsin-1, with three hydrogen bond interactions at Ile 223, Tyr 225, and Thr 222 at the active site of the enzyme followed by cedrane with  $-5.20$  kcal/mol.

#### PASS analysis

The bioactive compound 1,8 cineole underwent PASS (Prediction of Activity Spectra for Substances) and

ADMET (Absorption, Distribution, Metabolism, Excretion, and Toxicity) properties analysis, which are crucial for evaluating the therapeutic potential of a drug in living organisms (Wu et al., 2020). The drug-likeness was calculated by following the Lipinski rule of five (RO5), which states that a drug must have a log  $P$  value of  $\leq 5$ , H-bond acceptors  $\leq 10$ , H-bond donors  $\leq 5$ , and no more than one violation. It was observed that 1,8 cineole obeyed RO5. With 1,8 cineole, the number of H-bond acceptors was 1, and the H-bond donor was 0 (Table 4). The number of violations following RO5 was also 0. The Log  $P_{o/w}$  value ( $v$ ) for 1,8 cineole was determined to be 2.67. In pharmaco-analysis, Log  $P_{o/w}$  is a potential factor

Table 4. Physicochemical properties and pharmacokinetics properties of 1,8 cineole

Physicochemical properties	
Formula	C <sub>10</sub> H <sub>18</sub> O
Molecular weight	154.25 g/mol
Number of heavy atoms	11
Number of arom heavy atoms	0
Fraction Csp <sup>3</sup>	1.00
Number of rotatable bonds	0
Number of H-bond acceptors	1
Number of H-bond donors	0
Molar refractivity	47.12
TPSA	9.23 Å <sup>2</sup>
Lipophilicity	
Log <i>P</i> <sub>o/w</sub> (iLOGP)	2.58
Log <i>P</i> <sub>o/w</sub> (XLOGP3)	2.74
Log <i>P</i> <sub>o/w</sub> (WLOGP)	2.74
Log <i>P</i> <sub>o/w</sub> (MLOGP)	2.45
Log <i>P</i> <sub>o/w</sub> (SILICOS-IT)	2.86
Consensus Log <i>P</i> <sub>o/w</sub>	2.67
Pharmacokinetics	
GI absorption	high
BBB permeant	yes
P-gp substrate	no
CYP1A2 inhibitor	no
CYP2C19 inhibitor	no
CYP2C9 inhibitor	no
CYP2D6 inhibitor	no
CYP3A4 inhibitor	no
Log <i>K</i> <sub>p</sub> (skin permeation)	-5.30 cm/s
Druglikeness	
Lipinski	yes; 0 violation
Ghose	no; 1 violation: MW < 160
Veber	yes
Egan	yes
Muegge	no; 2 violations: MW < 200, heteroatoms < 2
Bioavailability Score	0.55
Medicinal chemistry	
PAINS	0 alert
Brenk	0 alert
Leadlikeness	no; 1 violation: MW < 250
Synthetic accessibility	3.65

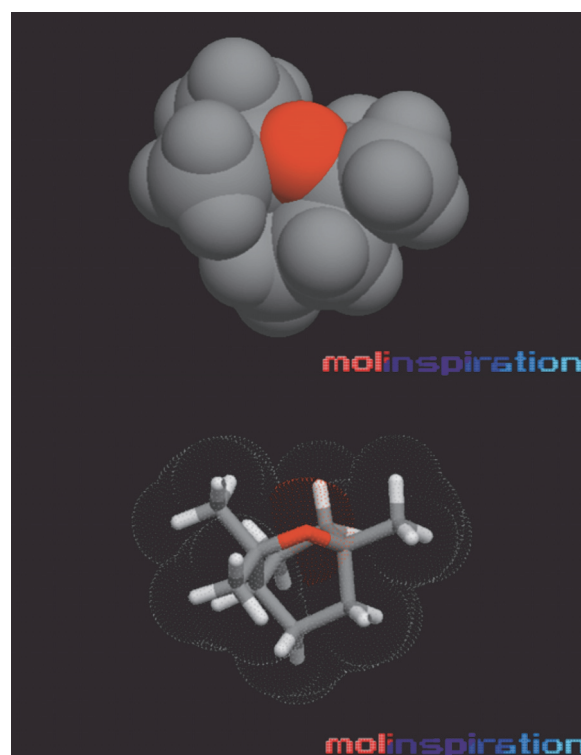


Fig. 3. Molecular lipophilicity potential (MLP)/polar surface area (PSA) views of 1,8 cineole; hydrophobic areas: encoded by violet; hydrophilic areas: red

Table 5. Bioactivity score of 1,8 cineole with different biological targets

Bioactivity	Score
Kinase inhibitor	-1.60
Nuclear receptor ligand	-1.07
GPCR ligand	-0.93
Protease inhibitor	-0.90
Enzyme inhibitor	-0.1
Ion channel modulator	0.01

to measure lipophilicity of any drug and its movement in the body after absorption (Abraham, 2003). Furthermore, it was observed that 1,8 cineole was a low molecular weight ligand (LMW) with a value of 154.25 g/mol. It is reported that ligands with low LMW possess a high tendency to transport across the cellular membranes and diffuse effortlessly compared to high MW compounds (Srimai et al., 2013). Molecular lipophilicity potential (MLP) depicting the surface view of eucalyptol is shown in Figure 3. The topological polar surface area (TPSA)

Table 6. Toxicity profile of 1,8 cineole

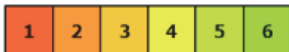
Classification	Target	Prediction
Toxicity endpoints	carcinogenicity	inactive
Toxicity endpoints	mutagenicity	inactive
Toxicity endpoints	cytotoxicity	inactive
Tox21-nuclear receptor signaling pathways	Aryl hydrocarbon Receptor (AhR)	inactive
Tox21-nuclear receptor signaling pathways	Androgen Receptor (AR)	inactive
Tox21-nuclear receptor signaling pathways	Androgen Receptor Ligand Binding Domain (AR-LBD)	inactive
Tox21-nuclear receptor signaling pathways	Peroxisome Proliferator-Activated Receptor Gamma (PPAR-Gamma)	inactive
Tox21-stress response pathways	Nuclear factor (erythroid-derived 2)-like 2/antioxidant responsive element (nrf2/ARE)	inactive
Tox21-stress response pathways	Heat Shock factor Response Element (HSE)	inactive
Tox21-stress response pathways	Mitochondrial Membrane Potential (MMP)	inactive
Tox21-stress response pathways	Phosphoprotein (Tumor Suppressor) p53	inactive
Tox21-stress response pathways	ATPase family AAA domain-containing protein 5 (ATAD5)	inactive
LD50	-	2100
$-\log_{10}(\text{LD}_{50})$	poison scale [0–13]	3.3
Predicted toxicity class		5

Table 7. Mycelial growth inhibition by EO against various fungal strains

Fungal culture	Sample volume used [ $\mu\text{l}/25\text{ml}$ ]	Mycelial growth inhibition [%]
MTCC 277	NC	NI
	50 $\mu\text{l}$	11 $\pm$ 1.2
	100 $\mu\text{l}$	55 $\pm$ 3.2
	ketoconazole	50 $\pm$ 2.0
MTCC 343	NC	NI
	50 $\mu\text{l}$	20 $\pm$ 1.0
	100 $\mu\text{l}$	50 $\pm$ 2.6
	ketoconazole	40 $\pm$ 3.3
MTCC 3373	NC	NI
	50 $\mu\text{l}$	67 $\pm$ 2.4
	100 $\mu\text{l}$	87 $\pm$ 4.3
	ketoconazole	50 $\pm$ 2.7

NC – negative control, NI – no inhibition

value was 9.23  $\text{\AA}^2$ , indicating that 1,8 cineole possesses good oral bioavailability (Biswal et al., 2019). TPSA is an important factor influencing drug transport properties like efficient permeability and absorption (Wu et al.,

2020). To exert toxic effects, the drug has to be absorbed thoroughly into the human body. As shown in Table 4, gastrointestinal tract (GI) absorption of 1,8 cineole was high (Table 4). Additionally, it was found that 1,8 cineole was a non-substrate for P-glycoprotein (P-gp) efflux transporters. In the human body, P-gp pumps drugs back into the lumen, lessening their absorption (Konig and Muller, 2013). Moreover, as shown in Table 4, 1,8 cineole was identified as a nonsubstrate for the CYP450 series of enzymes. In the human body, CYP450 enzymes are involved in liver detoxification (Srimai et al., 2013). These results indicate that 1,8 cineole can effectively target receptors and warrant further evaluation for its biological activity score.

Biological activity (BA) is a critical factor that determines the potential of a drug to bind to specific drugs or biological targets (Khan et al., 2017). In living systems, these biological targets usually include ion channels or biological receptors (Khan et al., 2017). According to the BA rule, a drug is considered active if its BA score is greater than 0, silent if it is less than  $-5.0$ , and sufficiently active if it falls between  $-5.0$  and 0 (Khan et al., 2017). As shown in Table 5, BA scores of 1,8 cineole for various targets are as follows:  $-1.60$  for kinase inhibitor,

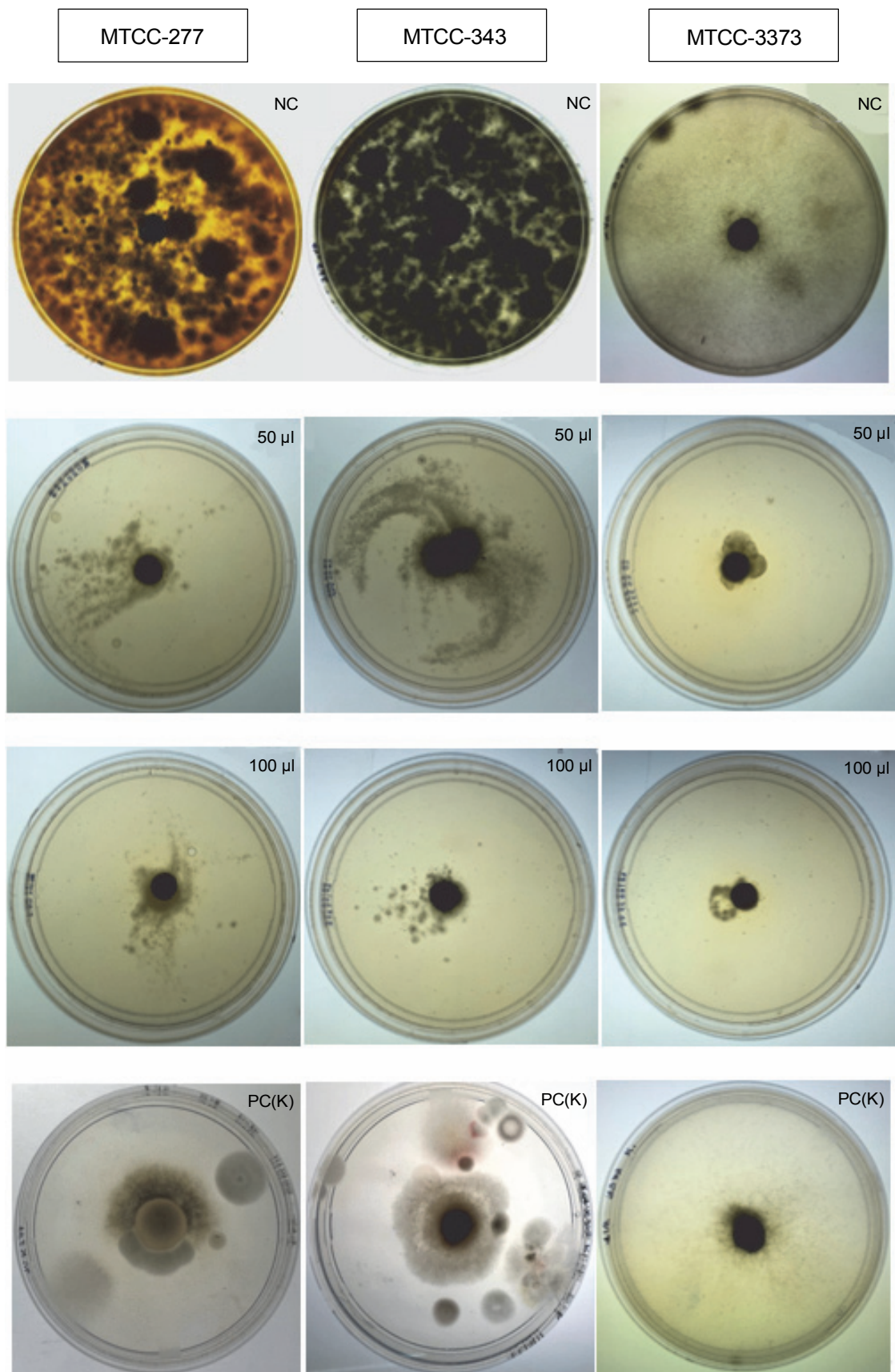


Fig. 4. Determination of antifungal activity of EO against various fungal strains PC(K) – positive control ketoconazole (25 µg/ml), NC – negative control

-1.07 for nuclear receptor ligand, -0.93 for GPCR ligand -0.90 for protease inhibitor, -0.1 for enzyme inhibitor, and 0.01 for ion channel modulator. It was observed that 1,8 cineole exhibited activity as an enzyme inhibitor and ion channel modulator. As for kinase inhibitors, nuclear receptor ligands, GPCR ligands, and protease inhibitors, the ligand demonstrated sufficient activity. These findings indicate that the studied bioactive compound possesses the necessary properties for it to potentially serve as a key drug (Khan et al., 2017). The bioactivity score provides valuable insights into the binding interactions of bioactive compounds, facilitating the development of new drugs with improved binding selectivity profiles and reduced undesired effects (Khan et al., 2017).

The toxicity profile of 1,8 cineole was calculated using the ProTox tool. To be used as an effective therapeutic drug in pharmaceutical companies, *in silico* toxicity analysis is a prerequisite (Banerjee et al., 2018). Raies et al. (2016) highlighted the importance of analyzing the toxicity profile of drugs to assess potential harm to humans, the environment, or animals. The toxicity profile of the ligand was assessed, and it revealed that 1,8 cineole was nontoxic, nonmutagenic, and noncarcinogenic (Table 6). Furthermore, the bioactive compound 1,8 cineole showed inactivity toward the biological pathways-based targets such as androgen receptor-ligand-binding domain (AR-LBD), aryl hydrocarbon receptor (AhR), androgen receptor, weak response element heat shock factor (HSE), nuclear factor (derived from erythroid 2)-antioxidant/antioxidant response factor (nrf2/ARE), and mitochondrial membrane potential (MMP) (Table 6). Lea et al. (2017) reported that the mutagenic nature of biologically active substances is harmful to cells and is the main driver behind several diseases, such as cancer. Huang et al. (2016) reported that all these targets are principal components of biological systems inside the human body. Furthermore, the prediction results revealed that 1,8 cineole belongs to toxicity class 5, indicating the safe nature of the bioactive compound (Table 6). LD50 is the toxic unit that measures the lethal toxicity dose of the drug; the predicted LD50 value was 2100 mg/kg for 1,8 cineole. On the toxic scale, the  $-\log_{10}(\text{LD}_{50})$  value of 1,8 cineole was 3.3, indicating its nontoxic nature. On the poison scale, which covers a range of 13 orders of magnitude, lower

$-\log_{10}(\text{LD}_{50})$  values indicate the nontoxic nature of drugs (Strey, 2019).

#### *In vitro* antifungal activity of EO

Wet lab authentication further corroborated the *in silico* findings by using three fungal strains, namely *A. niger* (MTCC 277), *A. oryzae* (MTCC 343), *Mucor* sp. (MTCC 3473). When using EO, at a concentration of 50  $\mu\text{l}$ , 67% mycelial growth inhibition was observed in MTCC 3473 fungal strain, whereas 11% and 20% mycelial growth inhibition was observed for MTCC 277 and MTCC 343, respectively (Fig. 4, Table 7). At a concentration of 100  $\mu\text{l}$ , the EO displayed 87% growth inhibition against MTCC 3473, 55% against MTCC 277, and 50% against MTCC 343. The antifungal potential of EO may be attributed to the presence of the major component, 1,8 cineole, or a combination of major and minor components. It is possible that the EO easily penetrates the fungal cell wall, leading to membrane leakage of electrolytes or lipid peroxidation of the membrane, which eventually hinders fungal hyphal growth and germination of conidia of fungal strains (Bakkali et al., 2008). It was also noted that certain antifungal agents inhibit fungal growth by interfering with ergosterol biosynthesis by binding to ergosterol in membranes. This damages the integrity and function of membrane-bound proteins and disturbs osmosis, fungal growth, and proliferation (Bendaha et al., 2011). Notably, this study reported 50–87% fungal inhibition by using 100  $\mu\text{l}$  of EO. Fungicidal effects at a concentration of 500  $\mu\text{l}$  of EO have also been pronounced for other pathogenic fungi, such as *Magnaporthe grisea* (81%), *Botrytis cinerea* (75%), *Bipolaris maydis* (62%), *Rhizoctonia solani* (46%), *Colletotrichum gloeosporioides* (45%), *Alternaria longipes* (31%), *Alternaria solani* (26%), and *Fusarium moniliforme* (25%) (Zhou et al., 2016). Similar findings have been reported by Hua et al. (2014) who studied litsea, anise, peppermint, camphor, and eucalyptus EOs and showed dose-dependent antifungal activity against *Aspergillus ochraceus*. The authors observed 50–70% inhibition of fungal growth rate at a concentration of 250–500  $\mu\text{l}$  of oils. Passone et al. (2012) reported the effect of boldo EO against *Aspergillus nigri* growth and observed that boldo EO showed the greatest effect on fungal isolates with significant growth reductions at 1000 and 2000  $\mu\text{l}$ , as well as total growth inhibition at

3000  $\mu\text{l}$ . *Matricaria chamomilla* L. oil was found to be a potent inhibitor of *A. niger* growth *in vitro*, with growth inhibition of  $\sim 7.5\%$  at 15.62  $\mu\text{l}$  and reaching a maximum of  $\sim 92.5\%$  at 1000  $\mu\text{l}$  (Tolouee et al., 2010).

## Conclusion

The aroma profile of the EO showed that 1,8 cineole was the major component, accompanied by some other minor components. The molecular docking study revealed that 1,8 cineole from EO was an effective ligand, which docked with fungal cell wall enzymes like RS, RibD, and DBPSG. Wet-lab results showed substantial inhibition of the growth of the fungal strains that cause aspergillosis and mucormycosis diseases. Therefore, the combined findings from the *in silico* and wet-lab experiments established that eucalyptus plant EO might be a promising antifungal therapeutic drug against aspergillosis and mucormycosis.

## Funding

This research was funded by the Department of Science and Technology, Government of India, no. DST/SEED/SCSP/STI/2019/253.

## References

- Abraham D.J. (2003) *Burger's medicinal chemistry and drug discovery*. Vol. 5: *Chemotherapeutic agents*.
- Alanio A., Dellièrè S., Fodil S., Bretagne S., Mégarbane B. (2020) *Prevalence of putative invasive pulmonary aspergillosis in critically ill patients with COVID-19*. *Lancet Respir. Med.* 8: e48–49.
- Averianova L.A., Balabanova L.A., Son O.M., Podvolotskaya A.B., Tekutyeva L.A. (2020) *Production of vitamin B2 (Riboflavin) by microorganisms: an overview*. *Front Bioeng. Biotechnol.* 12(8): 570828.
- Bakkali F., Averbeck S., Averbeck D., Idaomar M. (2008) *Biological effects of essential oils – a review*. *Food Chem. Toxicol.* 46: 446–475.
- Banerjee P., Eckert A.O., Schrey A.K., Preissner R. (2018) *ProTox-II: a webserver for the prediction of toxicity of chemicals*. *Nucl. Acids Res.* 46(W1): W257–W263.
- Barcellos M.P., Santos C.B., Federico L.B., Almeida P.F., da Silva C.H.T.P., Taft C.A. (2019) *Pharmacophore and structure-based drug design, molecular dynamics and admet/tox studies to design novel potential pad4 inhibitors*. *J. Biomol. Struct. Dyn.* 37: 966–981.
- Bendaha H., Yu L., Touzani R., Souane R., Giaever G. (2011) *New azole antifungal agents with novel modes of action: synthesis and biological studies of new tridentate ligands based on pyrazole and triazole*. *Eur. J. Med. Chem.* 46: 4117–4124.
- Bhatnagar A. (2018) *Composition variation of essential oil of Cymbopogon spp. growing in Garhwal region of Uttarakhand, India*. *J. App. Nat. Sci.* 10: 363–366.
- Biswal A.R., Venkataraghavan R., Pazhamalai V., Romauld S. (2019) *Molecular docking of various bioactive compounds from essential oil of Trachyspermum ammi against the fungal enzyme Candidapepsin-I*. *J. Appl. Pharma Sci.* 9: 21–32.
- Chang C.C., Senining R., Kim J., Goyal R. (2020) *An acute pulmonary coccidioidomycosis coinfection in a patient presenting with multifocal pneumonia with COVID-19*. *J. Investig. Med. High Impact Case Rep.* 8: 23247096209 72244.
- Chen X., Zewen Z., Zuozhong C., Yiman Li., Shan Su., Shujuan S. (2020) *Potential antifungal targets based on glucose metabolism pathways of Candida albicans*. *Front. Microbiol.* 11: 296.
- Cuenca-Estrella M. (2014) *Antifungal drug resistance mechanisms in pathogenic fungi: from bench to bedside*. *Clin. Microbiol. Infect.* 20: 54–59.
- Demuyser L., Palmans I., Vandecruys P., Van Dijck P. (2020) *Molecular elucidation of riboflavin production and regulation in Candida albicans, toward a novel antifungal drug target*. *mSphere* 5: e00714–e00720.
- Elaissi A., Bel Haj Salah K., Mabrouk S., Chemli R., Harzallah-Skhiri F. (2011) *Antibacterial activity and chemical composition of 20 Eucalyptus species essential oils*. *Food Chem.* 129: 1427–1434.
- Gakuubi M.M., Angeline W.M., Wagacha J.M. (2017) *Antifungal activity of essential oil of Eucalyptus camaldulensis Dehnh. against selected Fusarium spp.* *Int. J. Microbiol.* 2017: 8761610.
- Gangneux J.P., Bougnoux M.E., Dannaoui E., Cornet M., Zahar J.R. (2020) *Invasive fungal diseases during COVID-19: we should be prepared*. *J. Mycol. Med.* 30: 100971.
- Garg D., Muthu V., Sehgal I.S., Ramachandran R., Kaur H., Bhalla A., Puri G.D., Chakrabarti A., Agarwal R. (2021) *Coronavirus disease (Covid-19) associated mucormycosis (CAM): case report and systematic review of literature*. *Mycopathologia* 186: 289–298.
- Hua H., Xing F., Selvaraj J.N., Wang Y., Zhao Y., Zhou L., Liu X., Liu Y. (2014) *Inhibitory effect of essential oils on Aspergillus ochraceus growth and ochratoxin A production*. *PLoS One* 25: e108285.
- Huang R., Xia M., Sakamuru S., Zhao J., Shahane S.A., Attene-Ramos M., Zhao T., Austin C.P., Simeonov A. (2016) *Modelling the Tox21 10 K chemical profiles for in vivo toxicity prediction and mechanism characterization*. *Nat. Commun.* 7: 1–10.
- Jain C.K., Dasgupta A., Taneja N., Chaubey S., Gabrani R., Sharma S.K., Gupta S. (2013) *Putative drug targets in Rhizopus oryzae: in silico insight*. *Int. J. Bioinform. Res. Appl.* 9: 595–603.
- John T.M., Jacob C.N., Kontoyiannis D.P. (2021) *When uncontrolled diabetes mellitus and severe COVID-19 converge: the perfect storm for Mucormycosis*. *J. Fungi (Basel)* 15: 298.

- Khan T., Dixit S., Ahmad R. et al. (2017) *Molecular docking, PASS analysis, bioactivity score prediction, synthesis, characterization and biological activity evaluation of a functionalized 2-butanone thiosemicarbazone ligand and its complexes*. J. Chem. Biol. 10: 91–104.
- Konig J., Muller F. (2013) *Transporters and drug-drug interactions: important determinants of drug disposition and effects*. Pharmacol Rev. 65: 944–966.
- Kushwaha N., Chandra S., Singh C., Pharmacy K., Puramufit K., Kesharwani P.U. (2018) *A review on therapeutics application of Eucalyptus oil*. Int. J. Herbal Med. 6: 110–115.
- Lansbury L., Lim B., Baskaran V., Lim W.S. (2020) *Co-infections in people with COVID-19: a systematic review and meta-analysis*. J. Infect. 81: 266–275.
- Lawrence K., Lawrence R., Parihar D., Srivastava R., Charan A. (2012) *Antioxidant activity of palmarosa essential oil (Cymbopogon martini) grown in north indian plains*. Asian Pacific J. Tropical Dis. 2: S765–S768.
- Liao D.I., Wawrzak Z., Calabrese J.C., Viitanen P.V., Jordan D.B. (2001) *Crystal structure of riboflavin synthase*. Structure 9: 399–408.
- Lima S.L., Colombo A.L., de Almeida Junior J.N. (2019) *Fungal cell wall: emerging antifungals and drug resistance*. Front. Microbiol. 10: 2573.
- Madhavan Y., Sai K.V., Shanmugam D.K., Manimaran A., Guruviah K., Mohanta Y.K., Venugopal D.C., Mohanta T.K., Sharma N., Muthupandian S. (2022) *Current treatment options for COVID-19 associated mucormycosis: present status and future perspectives*. J. Clin. Med. 11: 3620.
- Omar H.S., Abd El-Rahman S.N., AlGhannam S.M., Sedeek M.S. (2021) *Antifungal evaluation and molecular docking studies of Olea europaea leaf extract, Thymus vulgaris and Boswellia carteri essential oil as prospective fungal inhibitor candidates*. Molecules 26: 6118.
- Passone M.A., Girardi N.S., Etcheverry M. (2012) *Evaluation of the control ability of five essential oils against Aspergillus section Nigri growth and ochratoxin A accumulation in peanut meal extract agar conditioned at different water activities levels*. Int. J. Food Microbiol. 159: 198–206.
- Raho G.B., Benali M. (2012) *Antibacterial activity of the essential oils from the leaves of Eucalyptus globulus against Escherichia coli and Staphylococcus aureus*. Asian Pac. J. Trop. Biomed. 2: 739–742.
- Raies A.B., Bajic V.B. (2016) *In silico toxicology: computational methods for the prediction of chemical toxicity*. Wiley Interdiscip. Rev. Comput. Mol. Sci. 6: 147–172.
- Schweer K.E., Bangard C., Hekmat K., Cornely O.A. (2014) *Chronic pulmonary aspergillosis external icon*. Mycoses 57: 257–270.
- Sebei K., Sakouhi F., Herchi W., Khouja M.L., Boukhchina S. (2015) *Chemical composition and antibacterial activities of seven Eucalyptus species essential oils leaves*. Biol. Res. 48: 7.
- Seyedjavadi S.S., Bagheri P., Nasiri M.J., Razzaghi-Abyaneh M., Goudarzi M. (2022) *Fungal infection in Co-infected patients with COVID-19: an overview of case reports/case series and systematic review*. Front. Microbiol. 13: 888452.
- Song G., Liang G., Liu W. (2020) *Fungal Co-infections associated with global COVID-19 pandemic: a clinical and diagnostic perspective from China*. Mycopathologia 185(4): 599–606.
- Srimai V., Ramesh M., Parameshwar K.S., Parthasarathy T. (2013) *Computer-aided design of selective Cytochrome P450 inhibitors and docking studies of alkyl resorcinol derivatives*. Med. Chem. Res. 22: 5314–5323.
- Strey K. (2019) *Die Gifte-Skala. Chemie in unserer Zeit*. 53: 386–399. <https://doi.org/10.1002/ciuz.201900828>
- Tolouee M., Alinezhad S., Saberi R., Eslamifar A., Zad S.J. (2010) *Effect of Matricaria chamomilla L. flower essential oil on the growth and ultrastructure of Aspergillus niger van Tieghem*. Int. J. Food Microbiol. 139: 127–133.
- Tyagi A.M., Bukvicki D., Gottardi D., Tabanelli G., Montanari C., Malik A., Guerzoni M.E. (2014) *Eucalyptus essential oil as a natural food preservative: in vivo and in vitro anti-yeast potential*. BioMed Res. Int. 2014: 969143.
- Ventoulis I., Sarmourli T., Amoiridou P., Mantzana P., Exindari M., Gioula G. (2020) *Bloodstream infection by Saccharomyces cerevisiae in two COVID-19 patients after receiving supplementation of Saccharomyces in the ICU*. J. Fungi (Basel). 6: 98.
- Wu C., Liu Y., Yang Y., Zhang P., Zhong W., Wang Y., Wang Q., et al. (2020) *Analysis of therapeutic targets for SARS-CoV-2 and discovery of potential drugs by computational methods*. Acta Pharm. Sinica B 10: 766–788.
- Zhou L.J., Li F.R., Huang L.J., Yang Z.R., Yuan S., Bai L.H. (2016) *Antifungal activity of eucalyptus oil against rice blast fungi and the possible mechanism of gene expression pattern*. Molecules 21(5): 621.